

# **Ion-Transfer Voltammetric Behaviour of Propranolol at Nanoscale Liquid-Liquid Interface Arrays**

Yang Liu,<sup>†</sup> Jörg Strutwolf,<sup>‡</sup> Damien W. M. Arrigan<sup>\*,†</sup>

<sup>†</sup>Nanochemistry Research Institute, Department of Chemistry, Curtin University, GPO Box U1987, Perth, Western Australia 6845, Australia

<sup>‡</sup>Institute of Organic Chemistry, University of Tübingen, Auf der Morgenstelle 18, 72076 Tübingen, Germany

**ABSTRACT:** In this work, the ion-transfer voltammetric detection of the protonated  $\beta$ -blocker propranolol was explored at arrays of nanoscale interfaces between two immiscible electrolyte solutions (ITIES). Silicon nitride nanoporous membranes with 400 pores in a hexagonal arrangement, with either 50 or 17 nm radius pores, were used to form regular arrays of nanoITIES. It was found that the aqueous-to-organic ion-transfer current continuously increased steadily rather than reaching a limiting current plateau after the ion transfer wave; the slope of this limiting current region was concentration dependent and associated with the high ion flux at the nanointerfaces. Electrochemical data were examined in terms of an independent nanointerface approach and an equivalent microdisc approach, supported by finite element simulation. In comparison to the larger interface configuration (50 nm radius), the array of 17 nm radius nanoITIES exhibited a 6.5-times higher current density for propranolol detection due to the enhanced ion flux arising from the convergent diffusion to smaller electrochemical interfaces. Both nanoITIES arrays achieved the equivalent limits of detection, 0.8  $\mu\text{M}$ , using cyclic voltammetry. Additionally, the effect of scan rate on the charging and faradaic currents at these nanoITIES arrays, as well as their stability over time, was investigated. The results demonstrate that arrays of nanoscale liquid-liquid interfaces can be applied to study electrochemical drug transfer, and provide the basis for the development of miniaturized and integrated detection platforms for drug analysis.

## Introduction.

Drug detection is of great importance in detection and control of substance misuse, abuse or addiction, as well as monitoring clinical effects of chronic diseases.<sup>1,2</sup> ( $\pm$ )-Propranolol hydrochloride is a  $\beta$ -blocker drug which is widely used to treat various cardiovascular disorders, such as angina pectoris, myocardial infarction and hypertension cardiac arrhythmias.<sup>3</sup> The rising demands for propranolol detection have driven tremendous efforts in the development of sensitive methods for quantification of propranolol in pharmaceutical formulations.<sup>4-8</sup> Among various analytical methods such as chromatographic and spectrophotometric analysis, electrochemical techniques have attracted considerable interest due to the high efficiency and low cost.<sup>9,10</sup> However, the direct oxidation of propranolol at conventional electrodes, including glassy carbon electrodes, requires high overpotentials. Therefore, many attempts have been made to modify electrodes with some catalytic materials such as carbon nanotubes<sup>11</sup> and copper-oxide nanoparticles<sup>12</sup>. Although lower overpotentials and higher sensitivity can be achieved, additional procedures to immobilize the catalytic materials on the electrodes are tedious but essential for the stability and reproducibility of the sensing platforms.<sup>13</sup>

Electrochemistry at the interface between two immiscible electrolyte solutions (ITIES) provides an alternative platform for label-free sensing of various ion species, ranging from inorganic to organic substances.<sup>14-16</sup> During recent decades, great efforts have been made to develop microITIES, which exhibited superior electrochemical properties such as reduced ohmic drop and enhanced mass transport, for both mechanistic study of ion-transfer reactions and sensing applications for molecules of biological importance.<sup>17-21</sup> Regarding propranolol detection, Collins *et al.* investigated the serum-protein effect on the voltammetric response of propranolol in a physiological matrix using the arrays of microITIES formed by silicon microporous membranes.<sup>22,23</sup> With the rapid development of nanotechnology, miniaturization of ITIES from microscale to nanoscale enables insights into behavior at liquid-liquid interfaces and opens up possibilities for improvement of sensitivity in electroanalytical applications.<sup>24,25</sup> Although nanoITIES arrays formed by multiple nanopores in parallel allow amplification of the electroanalytical signal, their analytical application is still embryonic and only model analyte ion transfers have been investigated.<sup>26-29</sup>

In this work, the behaviour of a drug based on ion-transfer voltammetry at nanoITIES arrays formed by silicon nitride nanoporous membranes was explored. The electrochemical behaviour of protonated propranolol transfer across the arrays of nanointerfaces (formed from nanopores of 50 or 17 nm radii) was investigated. A comparison was made of the analytical performances at these two nanoITIES arrays and the effect of ion flux on the steady-state current, which is different from that observed at microITIES, was examined. The electrochemical data are assessed in terms of simple

diffusion models and supported by finite element simulation. In addition, the effect of scan rate on the charging and faradaic currents obtained at these two nanoITIES arrays, as well as their stability over time were investigated.

## EXPERIMENTAL SECTION

### Reagents and Materials

All reagents were purchased from Sigma-Aldrich Australia, and used without further purification, unless stated otherwise. All aqueous solutions were prepared in ultrapure water (resistivity: 18 M $\Omega$  cm) obtained from a Milli-Q water purification system (Millipore Pty. Ltd., North Ryde, NSW, Australia). Both the aqueous and organic phases were mutually saturated before further use. The supporting electrolytes were lithium chloride (LiCl) in water and bis(triphenylphosphoranylidene)ammonium tetrakis(4-chlorophenyl)borate (BTPPATPBCl) in 1,6-dichlorohexane (1,6-DCH), both at a concentration of 10 mM. The organic electrolyte salt was prepared by metathesis reaction of bis(triphenylphosphoranylidene)ammonium chloride (BTPPACl) and potassium tetrakis(4-chlorophenyl)borate (KTPBCl) according to the published procedure.<sup>30</sup> The organic reference solution was 10 mM LiCl aqueous solution containing 10 mM BTPPACl.

The silicon nitride nanoporous membranes with thickness of 100 nm, prepared by combinations of photo- and electron-beam lithography, etching and deposition, were used to form the arrays of nanoITIES as described previously.<sup>26,29</sup> The arrays contain 400 pores (20  $\times$  20) arranged in a hexagonal pattern. As illustrated in the SEM images (Figure S1), two designs with pore radii of 50 and 17 nm were employed, and the pore-to-pore separation was 20 times the radius on each design.

### Experimental Procedure

Electrochemical experiments at nanopore-supported liquid-liquid interface arrays were performed on an Autolab PGSTAT 302N (Metrohm, The Netherlands) with ECD module. A two-electrode system composed of Ag|AgCl electrodes serving as both reference and counter electrode in either phase was housed in a Faraday cage to minimize electrical disturbance. The silicon chips (5 mm  $\times$  5 mm) containing the nanoporous arrays were affixed to a borosilicate glass tube holding approximately 100  $\mu$ L organic phase, and then it was immersed in 6 mL of the aqueous phase solution contained in a 10 mL glass beaker. The electrochemical cell can be summarized as follows:

Ag|AgCl|0.01 M LiCl<sub>w</sub> || 0.01 M BTPPATPBCl<sub>DCH</sub> | 0.01 M BTPPACl in 0.01 M LiCl<sub>w</sub> |AgCl|Ag

A background voltammogram was run over a wide potential range to establish the available potential window. Prior to the injection of analyte into the aqueous phase, a sequence of background voltammograms was recorded over a potential range large enough to encompass the transfer of the

analyte of interest. Then the stock solution of the analyte, prepared in DCH-saturated water containing 0.01 M LiCl, was added to the aqueous phase with a micropipette to produce the desired analyte concentration. In order to minimize and stabilize the background charging current, a quiet time of 5 s was implemented prior to recoding each voltammogram.

### **Simulations**

For the FEM simulations, the diffusion equation in two-dimensional cylindrical coordinates was numerically solved.<sup>31,32</sup> The simulations were performed using the commercial finite element modelling program COMSOL Multiphysics®, v. 3.5. A problem adapted mesh was created using free mesh parameters, as described previously.<sup>32</sup> Only diffusion of the analyte in the aqueous phase towards the interface was examined, neglecting transport within pore and any wall effects.

## **RESULTS AND DISCUSSION**

### **Voltammetric Behaviour of Propranolol**

Since the pH of the aqueous phase, 10 mM LiCl (pH ~6), was below the  $pK_a$  of propranolol ( $pK_a=9.23$ ),<sup>23</sup> the drug was protonated, which enabled it to transfer across and be detected at the nanoITIES. Figure 1A and 1B indicate the cyclic voltammetry (CV) of the electrolyte solutions in the absence and presence of propranolol (at concentrations of 20, 40, 60, 80 and 100  $\mu$ M) obtained with the arrays of 50 and 17 nm radius nanoITIES, respectively. These CVs show that the protonated propranolol commenced transfer from the aqueous phase to the organic phase at 0.6 V. The current increased steadily with applied potential up to the switching potential, but no true steady-state current plateau was reached in the diffusion-limited region, which is in agreement with previous reports on transfer of tetraethylammonium ( $TEA^+$ ) and tetrapropylammonium ( $TPrA^+$ ) cations across the water-DCH interface.<sup>27,29</sup> Furthermore, there was no reverse peak associated with the ions transferring back from the organic phase; this may be attributed to the complex behaviour resulting from multiple forces inside the nanopores, such as electrostatic, van der Waals or hydrophobic forces<sup>33-35</sup> or from mass transport effects.<sup>36</sup> This observation means that the stripping voltammetric technique, which was previously used to decrease the detection limit of propranolol at microITIES arrays, is not applicable to these arrays of nanoITIES. In addition, at the array of 17 nm radius nanoITIES, a current cross-over occurred when the concentration of propranolol increased to 60  $\mu$ M, which may be attributed to new phase formation, e.g. of an ion-pair precipitate.<sup>27</sup>

The background-subtracted voltammograms (forward scan only) of protonated propranolol transfer across arrays of 50 and 17 nm radius nanoITIES are shown in the insets of Figure 1A and 1B, respectively. In order to compare the response of these two nanoITIES arrays towards protonated

propranolol transfer, the current recorded at the potential ca. 200 mV positive of the foot of the ion transfer wave was determined as the experimental faradaic current, and the current density ( $J$ ) was calculated based on the geometric area of the nanopores. The resultant calibration plots of the current density at the arrays of 50 (circles) and 17 nm (squares) radius nanoITIES versus propranolol concentration are shown in Figure 1C. It can be observed that the slopes of these calibration plots, which indicate the analytical sensitivity of the nanoITIES, increased from 0.04 to 0.26 mA  $\mu\text{M}^{-1} \text{cm}^{-2}$  with the decrease of the nanointerface radius from 50 to 17 nm. This higher sensitivity towards protonated propranolol detection at smaller nanoITIES is attributed to the enhanced flux arising from convergent diffusion to smaller electrochemical interfaces.

Another interesting feature of the electrochemical behaviour of protonated propranolol transfer at the arrays of nanoITIES was that the current in the mass transport-limited region (above 0.8 V, Figure 1A and 1B) continued to increase with applied potential when the concentration of propranolol in the aqueous phase was greater than 20  $\mu\text{M}$ . Such behaviour has been observed before at nanoITIES arrays<sup>27</sup> at a concentration of 100  $\mu\text{M}$ ,

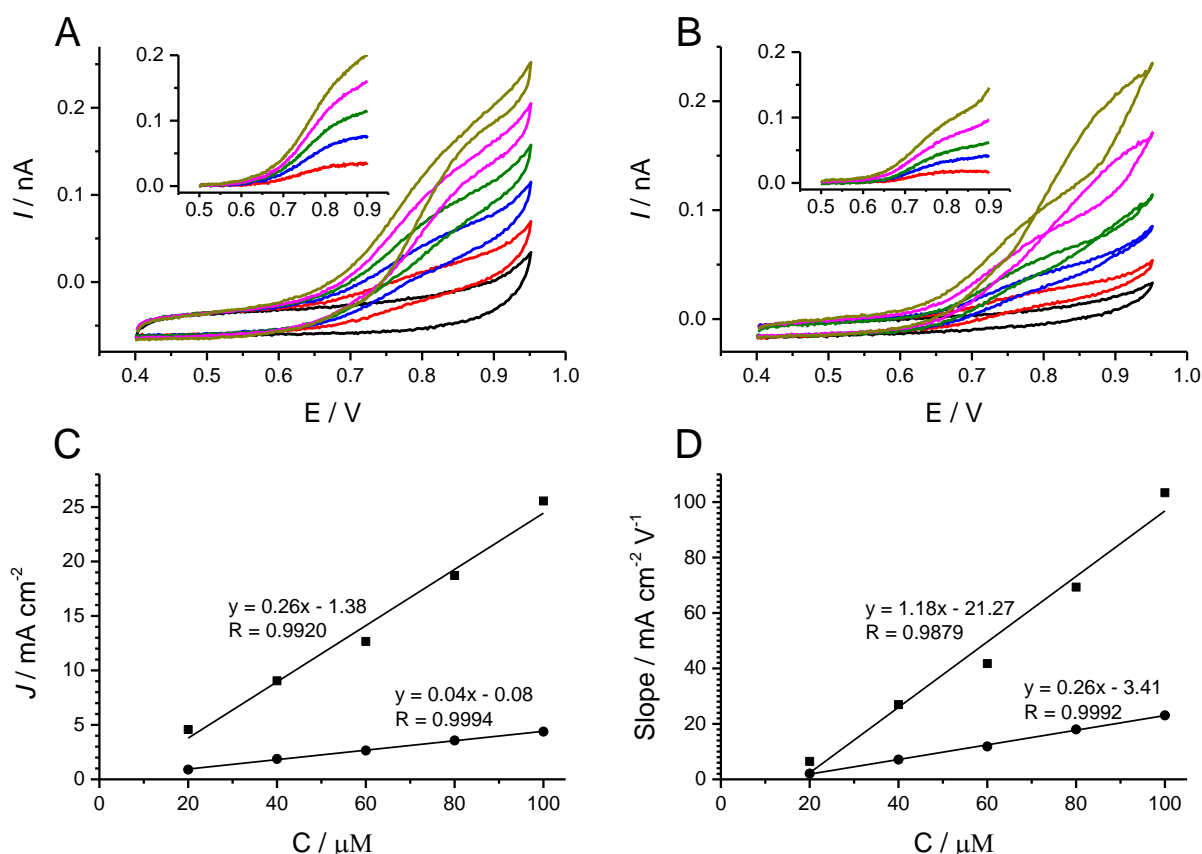


Figure 1. CVs of 0 (black), 20  $\mu\text{M}$  (red), 40  $\mu\text{M}$  (blue), 60  $\mu\text{M}$  (green), 80  $\mu\text{M}$  (pink) and 100  $\mu\text{M}$  (orange) protonated propranolol transfer across 50 (A) and 17 nm (B) radius nanoITIES arrays. The insets show the corresponding background-subtracted voltammograms. (C) Calibration plots of current density versus propranolol concentration (20-100  $\mu\text{M}$ ) obtained at 50 (circles) and 17 nm (squares) radius nanoITIES. (D) Slope of current density rise in the

potential range of 0.8-0.85 V versus propranolol concentration obtained at 50 (circles) and 17 nm (squares) radius nanoITIES. Scan rate: 5 mV s<sup>-1</sup>.

but this behaviour is different from that observed at microITIES arrays, where a clear steady-state current was reached.<sup>22</sup> Here, the slope of the current density rise between 0.8 and 0.85 V was examined as a function of the propranolol concentration in order to investigate the effect of the flux density on the voltammetric response at the nanoITIES arrays (Figure 1D). The results show that this slope was linearly dependent on the concentration of the transferring ion at these two nanoITIES arrays, and that the smaller nanointerfaces exhibited a more pronounced increase than the larger one. This suggested that the mass transport-controlled flux of protonated propranolol across the nanointerfaces has a significant effect on the limiting current obtained at the arrays of nanoITIES. To further explore the relationship between the ion transfer flux and limiting current at the arrays of small nanointerfaces, the background-subtracted voltammograms (forward scan only) of TPrA<sup>+</sup> transfer were also examined (Figure S2). As indicated, the slope of the current density rise in the range of 0.63-0.68 V increased linearly with the concentration in the range 20-100 μM, in agreement with the observation for protonated propranolol transfer. Therefore, the sloped nature of the current in the limiting current region at nanoITIES arrays is highly dependent on the ion flux across the nanointerfaces, which is associated with the concentration of the transferring analyte ions. It must also be pointed out that at lower concentrations, 20 μM in this case, the diffusion-limited current is a steady-state current, giving the expected sigmoidal voltammogram for radial diffusion control. At low flux (low concentrations of transferring species), the voltammogram is undisturbed and in agreement with the microITIES voltammogram shapes (radial diffusion). Hence, it appears that the ion flux leads to the sloping limiting current region.

### **Detection Limit of Propranolol**

To investigate the electrochemical performance of the nanointerface arrays for the detection of propranolol at low concentrations, the CVs of increasing propranolol concentration in the range 2-10 μM, in steps of 2 μM, were examined. Figure 2 shows the CVs and the insets show the corresponding background-subtracted voltammograms. It can be observed that the steady-state current can be achieved at both 50 and 17 nm nanointerfaces at these low concentrations, which further confirmed that a low ion flux provided stable limiting current at the nanoITIES arrays.

The detection limit, an important parameter to evaluate the performance capability of an electrochemical detection method, can be described as the analyte concentration which gives a faradaic signal significantly different from the background current.<sup>37</sup> Since the current reached a plateau at 0.8 V and the background noise was comparable to the faradaic signal for ion transfer at

low concentrations, the mean value of the currents recorded within the potential range 0.8-0.85 V, coupled with their standard deviations, were plotted against the concentration of propranolol (Figure 2C). The calculated detection limit (based on 3-times the standard deviation of the blank ( $3\sigma$ )) at both 50 and 17 nm radius nanoITIES arrays was 0.8  $\mu\text{M}$ . Therefore, regarding nanoITIES arrays, smaller nanointerfaces are promising candidates for the development of miniaturized detection platforms as they deliver similar high performances. Such detection limits for CV at ITIES are 5-10 times lower than values obtained at larger interfaces, whether on millimetre-scale or micrometre scale using CV<sup>25</sup> and indicate the enhanced detection capability that can be achieved by use of smaller interfaces.

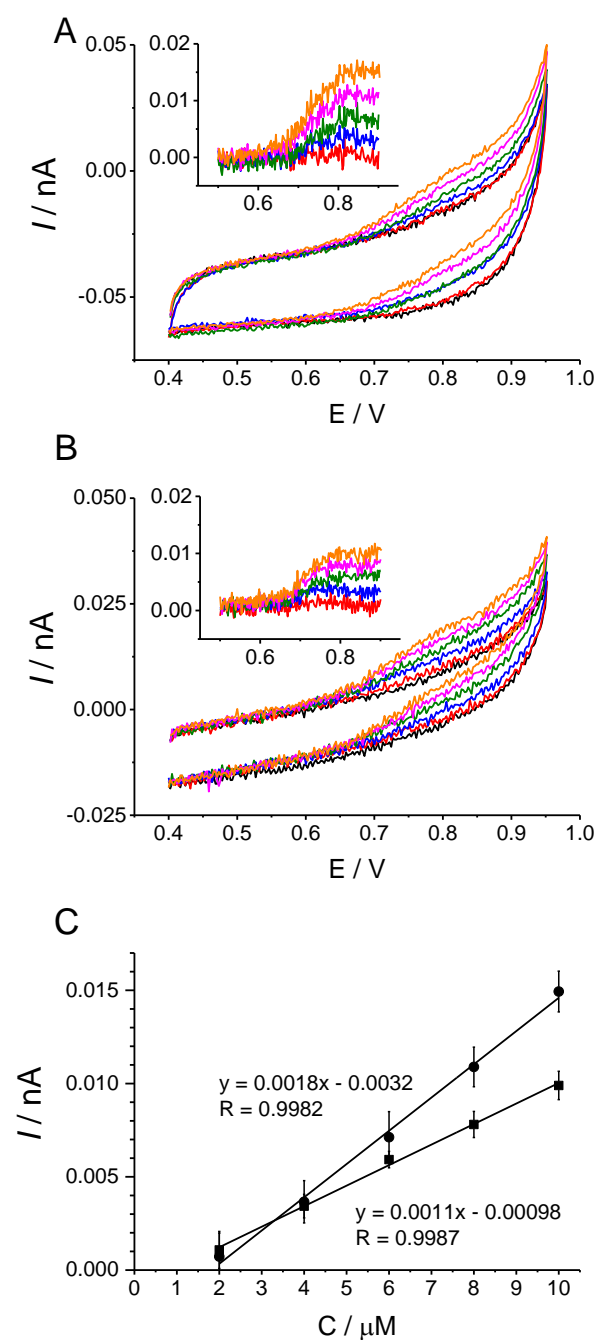


**Figure 2.** CVs of 0 (black), 2  $\mu\text{M}$  (red), 4  $\mu\text{M}$  (blue), 6  $\mu\text{M}$  (green), 8  $\mu\text{M}$  (pink) and 10  $\mu\text{M}$  (orange) protonated propranolol transfer across 50 (A) and 17 nm (B) radius nanoITIES arrays. (C) Calibration plots of current response versus propranolol concentration (2-10  $\mu\text{M}$ ) obtained at 50 (circles) and 17 nm (squares) radius nanoITIES. Scan rate: 5  $\text{mV s}^{-1}$ .

## Theoretical Analysis of the Limiting Currents

The ion-transfer current at the nanoITIES arrays can be examined by treating them as either an array of independent nanointerfaces or as a single microdisc interface of equivalent area. These approaches are called here the *independent nanointerfaces approach* and the *equivalent microdisc approach*, respectively.

*Independent nanointerfaces approach.* Theoretically, as each nanointerface in the array behaves like an inlaid disk electrode,<sup>27,29</sup> the steady-state current for an ion transferring from the aqueous to the organic phase is given by the Saito-Soos equation<sup>38,39</sup> multiplied by the number of pores,

$$I = N_p 4|z|FDc^b r_a \quad (1)$$

where  $I$  is the limiting current,  $z$ ,  $D$  and  $c^b$  are the charge, the diffusion coefficient and the bulk concentration of the transferred ion, respectively,  $F$  is the Faraday constant ( $96485 \text{ C mol}^{-1}$ ),  $r_a$  is the interface radius and  $N_p$  is the number of pores used to form the nanoITIES array,  $N_p=400$  for both arrays used in this work. For the transferring protonated propranolol ion,  $z = 1$  and  $D = 5 \times 10^{-10} \text{ m}^2 \text{ s}^{-1}$ .<sup>22</sup> This approach is valid if all 400 nanointerfaces behave independently, i.e. the diffusion field to each interface is not influenced by the diffusion field of the neighbouring interfaces. Therefore this is termed the *independent nanointerfaces approach*.

Using Equation (1), the theoretical values of the slopes of the current versus concentration plots at the arrays of 50 and 17 nm radius interfaces were 3.6 and 1.3  $\text{pA } \mu\text{M}^{-1}$ , respectively. In comparison, the experimental slopes at 50 and 17 nm radius nanointerface arrays (see Figure 2C) were 1.8 and 1.1  $\text{pA } \mu\text{M}^{-1}$ , which are ca. 50% and 85% of the theoretical values, respectively. The lower values of the experimental slopes (and hence the current) are due to the interactions of the diffusion zones formed at the nanointerfaces. If isolated, independent nanointerfaces were present, so that the diffusion zones around the individual interfaces do not interact, then larger currents in agreement with the prediction of Equation (1) would be obtained. However, with between-interface half-distances of 0.5  $\mu\text{m}$  and 0.17  $\mu\text{m}$  for the 50 nm and 17 nm radius nanointerface arrays, respectively, and the time scale of the experiments set by a relatively slow scan rate, the view of isolated pores is not valid. The local flux at a microdisc electrode is not uniform: it is highest at the electrode edge.<sup>40</sup> Analogously, the flux to each nanointerface depends on its position within the array, so that the interfaces are not equivalent. Therefore numerical simulations based on a diffusion zone approach to

quantitatively describe the array behaviour, as applied successfully to larger arrays of microinterfaces,<sup>32</sup> are not possible, because the diffusion zone approach requires equivalence of the interfaces within an array.<sup>32,41-43</sup> The numerical simulation of a microarray of electrodes or interfaces with interacting diffusion zones requires that the 3-dimensional nature of the array is taken into account (i.e. including the diffusional space). This is computationally expensive and only a few attempts have been made for arrays with much smaller numbers of electrodes<sup>44-47</sup> than used in the study presented here. A full 3-dimensional simulation for the 400 interfaces is not feasible. Although the diffusion zone domain approach is not applicable for the whole array, it might be useful to provide insight into the flux conditions for interfaces in the midst of the 400-interface array. Therefore FEM simulations for the 50 nm array (interface separation 1  $\mu\text{m}$ , hexagonal pattern) using the diffusion zone approach were performed.

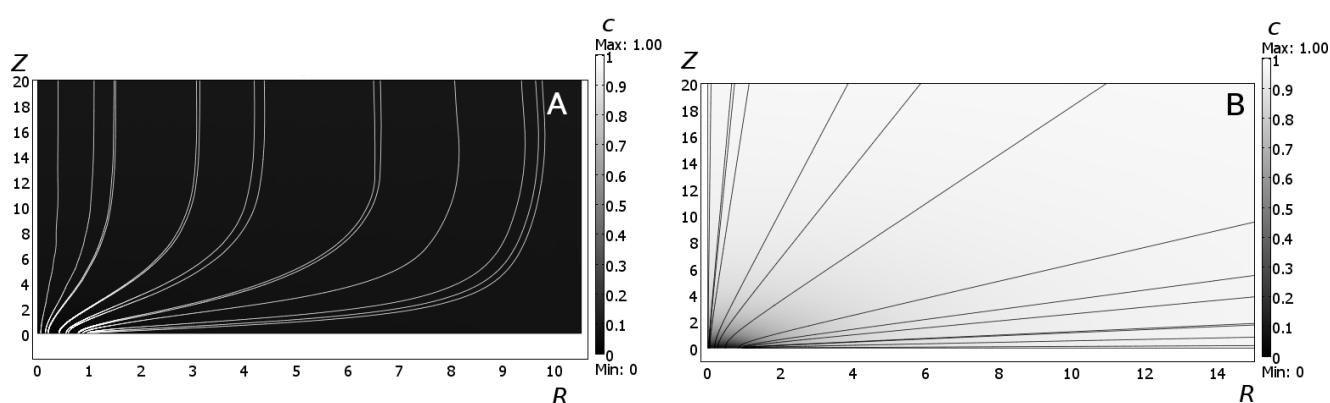


**Figure 3.** Simulated concentrations and analyte streamlines for a single 50 nm interface, **A** at the center of an array which has interface center-to-center distances 20-times the radius, and **B** an isolated pore. The duration of the diffusion process was 40 s for both cases. The grey-scale bars on the right-side of each plot indicate concentrations. In **A** the concentration is almost depleted; in **B** the depletion layer is restricted to the region close to the interface. The lines in **A** and **B** are streamlines of the analyte.

Figure 3A shows an area of the computational domain in the vicinity of the inlaid ITIES. The space is normalized by division with the interface radius,  $r_a$ , and the concentration by the bulk concentration. Therefore, the interface is located at ( $0 < R \leq 1$ ,  $Z=0$ ) and the dimensionless bulk concentration is one. The time of the concentration plots in Figure 3 is equivalent to 40 s for a 50 nm interface. This time corresponds to the time difference between 0.75 V, the  $E_{3/4}$  point (where, for a steady-state system, the interfacial concentration is zero), and the switching potential (0.95 V) at  $5 \text{ mV s}^{-1}$  scan rate. Due to the interaction of the diffusion zones and the resulting depletion of the analyte, the concentration in the region of solution between the interfaces has dropped to almost zero, as evident by the dark colour of the space. This means there is no radial diffusion to an interface located at the centre of the array. Figure 3A also contains the

analyte streamlines (which are perpendicular to the usually-shown equi-concentration lines), which show the path taken by the analyte ions as they follow the vector field of the concentration gradient. For distances in the  $Z$ -direction greater than *ca.* 10-times the interface radius, the stream lines run parallel to the  $Z$ -axis, indicating planar diffusion to an interface at the centre of the array. However, when approaching the interface, the analyte ions are "attracted" by the interface. For comparison, Figure 3B shows simulated concentrations at 40 s for a single isolated interface, where the diffusion zone can expand undisturbed, leading to a spherical diffusion field. Compared to Figure 3A, concentration depletion is only seen in close proximity to the ITIES. Clearly, the simulations show the dramatic impact of the surrounding nanointerface array on diffusion to a single nanointerface within the array. Consequently, because of the strong diffusion zone overlap and the decreased diffusional transport to the interfaces, Equation (1) overestimates the current.

*Equivalent disc approach.* Taking into consideration that the overall size of the nanointerface arrays are  $19.4 \times 16.5 \mu\text{m}^2$  for interface radius of 50 nm and  $5.8 \times 5.0 \mu\text{m}^2$  for the 17 nm interfaces, single discs of equivalent areas have a radii of 10 and 3  $\mu\text{m}$ , respectively. Therefore, for time scales of the experiments performed, the current responses of the arrays are expected to show the behaviour of microinterfaces, if no other complications are involved. Ideally, the CV experiment will lead to a sigmoidal curve with a steady-state limiting current. As a result, a micrometre-sized array of nanointerfaces will show the characteristics of a microinterface in a voltammetric experiment and the limiting current can be obtained from the Saito-Soos equation<sup>38,39</sup>

$$I = 4|z|FDc^b r_d \quad (2)$$

where now  $r_d$  is the radius of the disk with an area equivalent to the area covered by the nanointerface array. We refer to this as the *equivalent disk approach*. In the present case,  $r_d$  is 10 and 3  $\mu\text{m}$  for the arrays with 50 and 17 nm radius nanointerfaces, respectively. It should be kept in mind that the major part of the area of radius  $r_d$  is electrochemically inactive and the current flows only at the nanointerfaces (see streamlines in Figure 3A). For a hexagonal array where the center-to-center distance is 20 times the radius of the interfaces, the ratio of electroactive (conducting) to non-electroactive (insulating) areas is *ca.* 0.01. That is, the current density at the nanointerface array will be *ca.* 100-times higher than at a microdisc interface of equivalent size. The theoretical slope (Equation (2)) for the plot of limiting current versus the concentration using the *equivalent disk approach* is 1.9 pA  $\mu\text{M}^{-1}$  for the 50 nm interface array and 0.6 pA  $\mu\text{M}^{-1}$  for the 17 nm interface array. Table 1 lists the theoretical slopes for these plots calculated from Equation (1) (independent nanointerface approach) and Equation (2) (equivalent disc approach). Because of the assumed undisturbed diffusion to each nanointerface, the *independent nanointerface approach* gives an upper limit for the expected currents or slopes, while *the equivalent disk approach* gives a lower limit, caused by the total overlap of diffusion zones. The slopes calculated from the *independent nanopore approach* are *ca.* double those of the *equivalent disk approach*. Table 1 also presents the experimental values, which were

based on measurements at lower concentrations of protonated propranolol (2 to 10  $\mu\text{M}$ ) because they show a clear limiting current behaviour (Figure 2). The independent nanointerface approach clearly overestimates the slopes for the 50 nm array, while the equivalent disk approach shows satisfactory agreement for this array. In contrast, the experimental slope for the 17 nm array is close to that estimated by the independent nanointerface approach, while the equivalent disc approach underestimates it.

**Table 1. Experimental and calculated slopes of current versus concentration plots**

	Slope [ $\text{pA } \mu\text{M}^{-1}$ ]	
Experiment (low concentration)	$1.8 \pm 0.5^{\text{a}}$	$1.1 \pm 0.3^{\text{b}}$
Independent nanointerface approach	$3.6^{\text{a}}$	$1.3^{\text{b}}$
Equivalent disk approach	$1.9^{\text{a}}$	$0.6^{\text{b}}$

<sup>a</sup> interface radius 50 nm; <sup>b</sup> interface radius 17 nm

### Scan Rate Studies

Besides the analytical performances of the arrays of 50 and 17 radius nanointerfaces towards propranolol detection, the effect of scan rate on both charging and faradaic current was investigated to understand the electrochemical properties of these nanoITIES arrays. Figure 4A and 4B indicate the effect of scan rate on the current response of 50 and 17 nm radius nanointerface arrays, respectively. The charging current was estimated from half of the difference between forward and reverse currents at the potential of 0.5 V, where no ion transfer occurred. It can be observed that the charging current ( $I_c$ ) increased linearly with the scan rate ( $\nu$ ) ranging from 3 to 30 mV/s (left hand side axis, circles) on both nanoITIES arrays.

As reported, the experimental capacitance ( $C_{\text{expt}}$ ), attributed to several capacitors present in the nanoITIES system such as electrical double layers formed at liquid-liquid and solid-liquid interfaces and silicon nitride membrane sandwiched between two electrolyte solutions, can be described as follows:<sup>29,48</sup>

$$C_{\text{expt}} = \frac{I_c}{\nu} \quad (3)$$

Therefore, the  $C_{\text{expt}}$  of the nanoITIES array systems with 50 and 17 nm radius nanointerfaces was calculated to be  $3.3 \pm 1.5$  and  $1.7 \pm 0.8$  nF, respectively, based on the slopes of the linear plots. These values were in

agreement with the previous data of 4.44 and 1.57 nF obtained at the arrays of 50 and 17 nm radius nanoITIES, respectively.<sup>29</sup>

In order to study the effect of scan rate on the faradaic current for protonated propranolol transfer across the arrays of nanoITIES, the concentration of 20  $\mu\text{M}$  was applied, since the faradaic current for ion transfer at lower concentrations may be obscured by the charging current at higher scan rates, and higher concentrations of transferring ion will lead to the sloping current rise instead of a steady-state current, as described above and in Figure 1A and 1B. The insets of Figure 4 indicate the CVs in the absence and the presence of 20  $\mu\text{M}$  propranolol recorded at the nanoITIES arrays using the scan rate of 3 (upper left) and 30 mV/s (bottom right). The faradaic currents for protonated propranolol transfer across the nanointerfaces were acquired based on the background-subtracted voltammograms. Here, the mean currents obtained within the potential range 0.8-0.85 V, coupled with their standard deviations, were plotted against the scan rate in the range 3-30 mV/s (Figure 4, right hand side axis, squares). As indicated, the faradaic current arising from protonated propranolol transfer across the arrays of nanoITIES is independent of the scan rate, as expected for a radial diffusion mass transfer.<sup>17</sup>

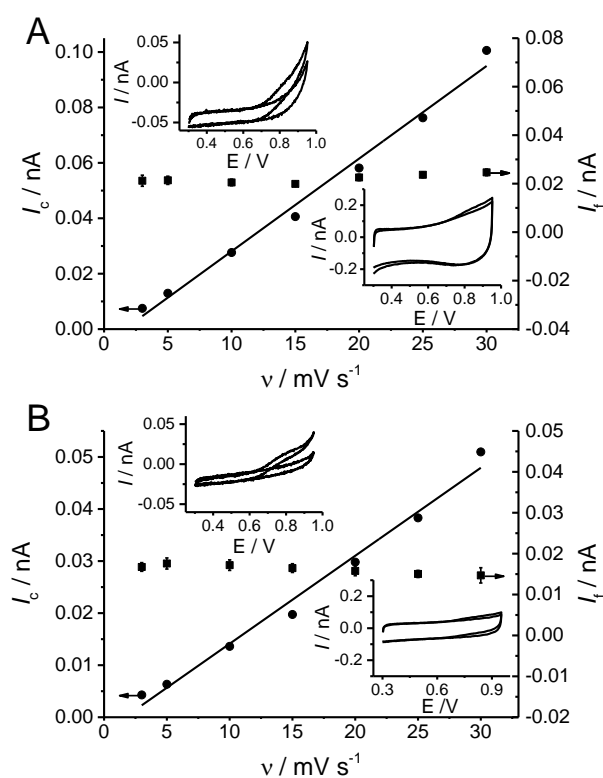


**Figure 4.** The effect of scan rate on the charging current (circles) and faradaic current for propranolol transfer (squares) obtained at the 50 (A) and 17 nm (B) radius nanoITIES. The insets show the corresponding CVs recorded at the nanoITIES arrays in the absence and presence of 20  $\mu\text{M}$  propranolol at the scan rate of 3 (upper left) and 30 mV s<sup>-1</sup> (lower right).

## Stability Studies

The stability of the nanoITIES arrays, which is an important parameter for applicability to electrochemical sensors, was investigated by monitoring both charging and faradaic currents for protonated propranolol transfer at the arrays of 50 and 17 nm radius nanointerfaces during one month period. Figure 5A indicates the change of charging current of these nanoITIES arrays over time. Again, the charging current was estimated from half of the difference between forward and backward currents in CVs recorded in blank electrolyte solutions at a potential of 0.5 V, where no ion transfer occurred. The relative standard deviation (RSD) was 12% and 15% for the 50 nm (circles) and 17 nm (squares) radius nanointerface arrays, respectively, based on 15 measurements in one month.

Regarding the stability of the faradaic current, five measurements of 100  $\mu\text{M}$  propranolol transfer across the nanoITIES arrays were carried out (Figure 5B). The arrays of 50 and 17 nm radius nanoITIES exhibited the RSDs of 2% and 7%, respectively, which are acceptable for practical sensing applications. In addition, the nanoITIES arrays formed by smaller pores showed greater relative variation than that of the larger pores.

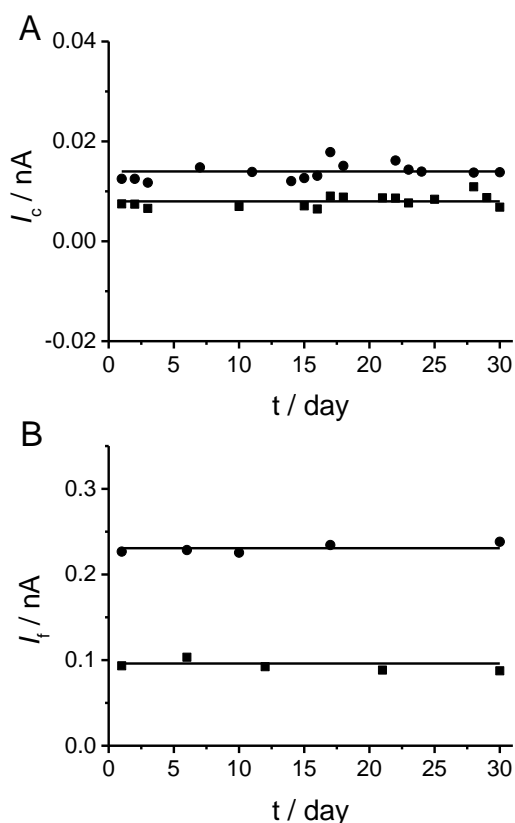


**Figure 5.** The stability of the charging current (A) and faradaic current for propranolol transfer (B) at the arrays of 50 (circles) and 17 nm (squares) radius nanoITIES.

## CONCLUSION

The voltammetric behavior of propranolol has been undertaken at water-1,6-dichlorohexane nanointerface arrays formed by silicon nitride membranes with two different nanopore designs (nanopore radii of 50 and 17 nm). By comparison, the smaller nanoITIES with radius of 17 nm exhibited higher sensitivity towards protonated propranolol transfer than the larger one with radius of 50 nm, which can be attributed to the enhanced ion flux resulting from the convergent diffusion at smaller electrochemical interfaces. Both nanoITIES arrays achieved the same limit of detection for propranolol detection, which makes the smaller nanoITIES a promising candidate for miniaturized sensing platforms with high efficiency and low cost. In addition, it was found that the electrochemical behaviour of protonated propranolol transfer across the arrays of nanoITIES was different from that of microITIES, as the diffusion current continuously increased instead of reaching a steady state plateau when high ionic flux was applied. However, at low concentrations of protonated propranolol the voltammograms exhibit a well defined steady-state limiting current. For a separation between interfaces of 20-times the interface radius, strong diffusion zone overlap occurs, leading to depletion zones between neighbouring nanointerfaces. This behaviour is illustrated by FEM simulation of an interface in the midst of the array. The limiting current of the array is therefore better described by an *equivalent disk approach* than by an *independent nanointerfaces approach*, as a comparison between experimental and calculated sensitivities show.

The reasons for the current increase associated with the ion transfer across nanoITIES arrays, shown here to be flux-dependent, remain the subject of investigations, as do improvements in the detection sensitivity of the nanoITIES systems for drug analysis.

## **ASSOCIATED CONTENT**

### **Supporting Information**

This material is available free of charge via the Internet at <http://pubs.acs.org>.

## **AUTHOR INFORMATION**

### **Corresponding Author**

\* E-mail: [d.arrigan@curtin.edu.au](mailto:d.arrigan@curtin.edu.au). Fax: +61892662300. Phone: +61892669735.

### **Author Contributions**

All authors have given approval to the final version of the manuscript.

## **ACKNOWLEDGMENT**

This work was supported by Australian Research Council (DP130102040). The authors acknowledge the use of equipment, scientific and technical assistance of the Curtin University Electron Microscope Facility, which is partially funded by the University and by the State and Commonwealth Governments, and thank Tyndall National Institute, Cork, Ireland, for the gift of the nanopore array membranes used.

## REFERENCES

- (1) Eliasson, E.; Lindh, J. D.; Malmstrom, R. E.; Beck, O.; Dahl, M. L. *Eur. J. Clin. Pharmacol* **2013**, *69*, S25-S32.
- (2) Gilbert, J. W.; Wheeler, G. R.; Mick, G. E.; Storey, B. B.; Herder, S. L.; Richardson, G. B.; Watts, E.; Gyarteng-Dakwa, K.; Marino, B. S.; Kenney, C. M.; Siddiqi, M.; Broughton, P. G. *Pain Physician* **2010**, *13*, 167-186.
- (3) Oliveira, G. G.; Azzi, D. C.; Vicentini, F. C.; Sartori, E. R.; Fatibello-Filho, O. *J. Electroanal. Chem.* **2013**, *708*, 73-79.
- (4) Sanghavi, N. M.; Jivani, N. G. *Talanta* **1980**, *27*, 591-592.
- (5) Ray, K.; Trawick, W. G.; Mullins, R. E. *Clin. Chem.* **1985**, *31*, 131-134.
- (6) Zahalka, L.; Matysova, L.; Sklubalova, Z.; Klovrvzova, S.; Solich, P. *Chromatographia* **2013**, *76*, 1553-1558.
- (7) Divya, O.; Shinde, M. *J. Appl. Spectrosc.* **2013**, *80*, 326-334.
- (8) Satinsky, D.; Havlikova, L.; Solich, P. *Anal. Bioanal. Chem.* **2013**, *405*, 6583-6587.
- (9) Bai, X.; You, T.; Sun, H.; Yang, X.; Wang, E. *Electroanalysis* **2000**, *12*, 535-537.
- (10) Gimenes, D. T.; Marra, M. C.; Abarza Munoz, R. A.; Angnes, L.; Richter, E. M. *Anal. Methods* **2014**, *6*, 3261-3267.
- (11) Zhao, K.; Yue, S.; Tian, D.; Zhang, Y. *J. Electroanal. Chem.* **2013**, *709*, 99-105.
- (12) Shadjou, N.; Hasanzadeh, M.; Saghatforoush, L.; Mehdizadeh, R.; Jouyban, A. *Electrochim. Acta* **2011**, *58*, 336-347.
- (13) Liu, Y.; Zhang, L.; Guo, Q.; Hou, H.; You, T. *Anal. Chim. Acta* **2010**, *663*, 153-157.
- (14) Girault, H. H. In *Electroanalytical Chemistry*, Bard, A. J.; Zoski, C. G., Eds.; CRC Press: New York, 2010, pp 1-104.
- (15) Liu, S.; Li, Q.; Shao, Y. *Chem. Soc. Rev.* **2011**, *40*, 2236-2253.
- (16) Reymond, F.; Fermin, D.; Lee, H. J.; Girault, H. H. *Electrochim. Acta* **2000**, *45*, 2647-2662.
- (17) Campbell, J. A.; Girault, H. H. *J. Electroanal. Chem.* **1989**, *266*, 465-469.
- (18) Taylor, G.; Girault, H. H. *J. Electroanal. Chem.* **1986**, *208*, 179-183.
- (19) Liu, B.; Mirkin, M. V. *Electroanalysis* **2000**, *12*, 1433-1446.
- (20) Herzog, G.; Beni, V. *Anal. Chim. Acta* **2013**, *769*, 10-21.
- (21) Alvarez de Eulate, E.; Arrigan, D. W. M. *Anal. Chem.* **2012**, *84*, 2505-2511.
- (22) Collins, C. J.; Arrigan, D. W. M. *Anal. Chem.* **2009**, *81*, 2344-2349.
- (23) Collins, C. J.; Lyons, C.; Strutwolf, J.; Arrigan, D. W. M. *Talanta* **2010**, *80*, 1993-1998.
- (24) Amemiya, S.; Wang, Y.; Mirkin, M. V. In *Electrochemistry*, Wadhawan, J. D., Compton, R. G., Ed.; Royal Society of Chemistry: Cambridge, 2013, pp 1-43.

- (25) Arrigan, D.; Herzog, G.; Scanlon, M.; Strutwolf, J. In *Electroanalytical Chemistry*, Bard, A. J.; Zoski, C., Eds.; Taylor and Francis: Hoboken, 2013, pp 105-178.
- (26) Scanlon, M. D.; Strutwolf, J.; Blake, A.; Iacopino, D.; Quinn, A. J.; Arrigan, D. W. M. *Anal. Chem.* **2010**, *82*, 6115-6123.
- (27) Rimboud, M.; Hart, R. D.; Becker, T.; Arrigan, D. W. M. *Analyst* **2011**, *136*, 4674-4681.
- (28) Scanlon, M. D.; Arrigan, D. W. M. *Electroanalysis* **2011**, *23*, 1023-1028.
- (29) Sairi, M.; Strutwolf, J.; Mitchell, R. A.; Silvester, D. S.; Arrigan, D. W. M. *Electrochim. Acta* **2013**, *101*, 177-185.
- (30) Lee, H. J.; Beattie, P. D.; Seddon, B. J.; Osborne, M. D.; Girault, H. H. *J. Electroanal. Chem.* **1997**, *440*, 73-82.
- (31) Britz, D. *Digital Simulation in Electrochemistry*, 3rd ed. ed.; Springer Berlin Heidelberg, 2005.
- (32) Strutwolf, J.; Scanlon, M. D.; Arrigan, D. W. M. *Analyst* **2009**, *134*, 148-158.
- (33) Segerink, L. I.; Eijkel, J. C. *Lab Chip* **2014**, *14*, 3201-3205.
- (34) Schoch, R.; Han, J.; Renaud, P. *Rev. Mod. Phys.* **2008**, *80*, 839-883.
- (35) Eijkel, J. C. T.; Berg, A. v. d. *Microfluid. Nanofluid.* **2005**, *1*, 249-267.
- (36) Chen, S. L.; Kucernak, A. *J. Phys. Chem. B* **2002**, *106*, 9396-9404.
- (37) Miller, J. C.; Miller, J. N. *Statistics for Analytical Chemistry*, 2nd ed.; Ellis Horwood: 1988.
- (38) Soos, Z. G.; Lingane, P. J. *J. Phys. Chem.* **1964**, *68*, 3821-3828.
- (39) Saito, Y. *Rev. Polarog.* **1968**, *15*, 177-187.
- (40) Oldham, K. B. *J. Electroanal. Chem. Interfacial Electrochem.* **1981**, *122*, 1-17.
- (41) Scheller, F.; Muller, S.; Landsber, R.; Spitzer, H. J. *J. Electroanal. Chem.* **1968**, *19*, 187-198.
- (42) Gueshi, T.; Tokuda, K.; Matsuda, H. *J. Electroanal. Chem.* **1978**, *89*, 247-260.
- (43) Amatore, C.; Saveant, J. M.; Tessier, D. *J. Electroanal. Chem.* **1983**, *147*, 39-51.
- (44) Godino, N.; Borrise, X.; Xavier Munoz, F.; Javier del Campo, F.; Compton, R. G. *J. Phys. Chem. C* **2009**, *113*, 11119-11125.
- (45) Zoski, C. G.; Wijesinghe, M. *Isr. J. Chem.* **2010**, *50*, 347-359.
- (46) Kolev, S. D.; Simons, J. H. M.; Vanderlinden, W. E. *Anal. Chim. Acta* **1993**, *273*, 71-80.
- (47) Fernandez, J. L.; Wijesinghe, M.; Zoski, C. G. *Anal. Chem.* **2015**, *87*, 1066-1074.
- (48) Vanýsek, P. *ECS Trans.* **2012**, *41*, 15-24.